SACLANTCEN REPORT
serial no.: SR-144

SACLANT UNDERSEA
RESEARCH CENTRE

REPORT

Results on the detection of narrow-band low-level signals in a ship-induced noise field using high-resolution beamforming

S. Jesus and
R.M. Heitmeyer

July 1988

The SACLANT Undersea Research Centre provides the Supreme Allied Commander Atlantic (SACLANT) with scientific and technical assistance under the terms of its NATO charter, which entered into force on 1 February 1963. Without prejudice to this main task—and under the policy direction of SACLANT—the Centre also renders scientific and technical assistance to the individual NATO nations.

SACLANTCEN SR-144

Results on the detection of narrow-band low-level signals in a ship-induced noise field using high-resolution beamforming

S. Jesus and R.M. Heitmeyer

The content of this document pertains to work performed under Project 21 of the SACLANTCEN Programme of Work. The document has been approved for release by The Director, SACLANTCEN.

Peter C. Wille
Director

Intentionally blank page

Results on the detection of narrow-band low-level signals in a ship-induced noise field using high-resolution beamforming

S. Jesus and R.M. Heitmeyer

Abstract: In this report the performance of a high-resolution beamformer is compared to that of the conventional beamformer in detecting a low-level narrow-band signal in the vicinity of a number of high-level noise sources. This scenario may arise in areas where shipping noise is predominant, the acoustic field being dominated to a large part by the contributions of individual ships. In this study a comparative detection performance test is conducted with a simulated source embedded in a real ship-induced noise field and received on a 64-element towed array. The results shown suggest that in such noise fields the detection performance of the conventional planewave beamformer is greatly reduced due to a lack of resolving power. High-resolution techniques may overcome this difficulty and a detection improvement of 5% to 20% is obtained in the detection of a low-level target in the frequency range below 250 Hz. When the signal-to-noise ratio increases the performance of both algorithms is comparable.

Keywords: detection o high-resolution beamforming o shipping noise

Contents

1. Introduction 1
2. Description of the algorithms 2
2.1. Conventional beamformer 3
2.2. High-resolution beamformer 3
3. Methodology of detection 5
4. Results 8
5. Conclusion 13

References 14

Appendix A - WB^3 algorithm equation flowchart 15

1. Introduction

For a conventional planewave beamformer an increase in the array length results in an increase in the signal-to-noise ratio gain and hence an increase in the detection performance. If the noise field is formed by a single point source in spatially white gaussian noise then the conventional beamformer is the optimum beamformer and the increase in the signal-to-noise ratio gain is the only benefit of increased aperture length.

For ship-induced noise fields, where the noise is largely due to the contribution of individual ships, an increase in the array length also results in an increase in the extent to which the contributions from the individual ships are resolved in steering angle. Thus, for ship-induced noise fields, increasing the aperture length affects detection performance, not only by increasing the array gain but also by increasing the extent to which noise sources are resolved. In such noise fields the limited resolution power of the conventional beamformer may lead to a situation where low-level sources may be masked by nearby high-level sources. Over the past two decades a number of high-resolution spatial array processing algorithms have been developed to improve the ability of sonar systems to angularly resolve closely-spaced sources [1-5]. For ship-induced noise fields these algorithms may offer an alternative to increasing the aperture length. An overview and comparative simulated study of the best-known high-resolution techniques applied to underwater acoustics can be found, for example, in [6]. The Ambient Noise Group (ANG) at SACLANTCEN has been involved in developing and testing such techniques to improve angular resolution of short linear towed arrays for horizontal noise directionality measurements [7,8].

In this report, we present an experimental evaluation of the detection performance of a high-resolution beamformer compared to that of the conventional planewave beamformer. The high-resolution technique used in the evaluation is the WB^3 algorithm developed by J.-L. Berrou as a modification of the WB^2 described in Wagstaff et al. [8]. Our choice of the WB^3 algorithm was largely motivated by data-processing considerations rather than performance considerations. The results are described by receiver operating characteristics (ROC) curves (probability of detection *vs* probability of false alarm) obtained both for the high-resolution and conventional beamformers.

The data used for the experimental detection evaluation is the high-resolution database acquired during the ANG cruise 1/84 in the Gulf of Genova. The choice of this working area was motivated by the high concentration of merchant ship traffic. This database provides a relatively long time record of data from a 64-hydrophone towed array with a known controlled multitone source signal embedded in ship-dominated noise.

2. Description of the algorithms

The detection performance evaluation is obtained by means of a conventional detection algorithm operating on a time series of frequency–wavenumber estimates computed by either the conventional beamformer or the high-resolution beamformer. Each frequency–wavenumber estimate is in turn computed in the conventional manner as a time-average of the two-dimensional FFT of the array sensor outputs. Thus the N-averaged frequency–wavenumber estimate at discrete frequency f_k and wavenumber κ_n at time t is computed according to

$$B(f_k, \kappa_n, t) = N^{-1} \sum_{m=1}^{N} B(f_k, \kappa_n, t_m), \tag{1a}$$

where the 'unaveraged' frequency–wavenumber estimate at time t_m is given by

$$B(f_k, \kappa_n, t_m) = \left| N_b^{-1} \sum_{l=0}^{N_b-1} h(l) Y_l(f_k, t_m) \exp[j2\pi\kappa_n l] \right|^2, \tag{1b}$$

where $Y_l(f_k, t_m)$ is the complex amplitude of the lth hydrophone output at frequency f_k and time 'snapshot' t_m, $h(l)$ is the spatial shading function, and N_b is the number of beams. The complex hydrophone amplitudes are obtained from a time-to-frequency fourier transform on the data acquired over the recording interval $[t_m - T_r, t_m]$. The discrete frequencies f_k with $k = 1, \ldots, K$ take on equally-spaced values in the frequency band of interest with a frequency spacing $\Delta f = T_r^{-1}$. The discrete normalized wavenumbers κ_n take on the values

$$\kappa_n = n/N_b, \quad n = 1, \ldots, N_b - 1, \tag{2}$$

where the number of beams N_b is an integer multiple of the number of hydrophones N_p. If $N_b > N_p$ the spatial shading function is $h(l) = 0$ with $l = N_p + 1, \ldots, N_b$ (zero padding).

2.1. CONVENTIONAL BEAMFORMER

The conventional beamformer operates on the array by coherent summation of the N_p sensor outputs (for a given frequency f_k) with the appropriate phase shifts to steer a 'beam' n to direction θ_n. This is done by identifying the normalized wavenumbers of (2) with the beam steering angles defined by the relationship

$$\theta_n = \arcsin\left[-\frac{f_d}{f_k} + 2\frac{f_d}{f_k}\kappa'_n\right], \tag{3}$$

where $\theta_n \in [-90°, 90°]$ and $\kappa'_n = (n-1)/N_b \in [0,1]$ for $n = 1, \ldots, N_b$ if the array design frequency $f_d = c/2d \geq f_k$ which is the case in this report.

- For $f_k = f_d$ the direction $\theta_1 = -90°$ corresponds to the aft endfire beam, the direction $\theta_{(N_b+1)/2} = \arcsin(-N_b^{-1})$ corresponds to the broadside beam and the direction $\theta_{N_b} = \arcsin(1 - 2N_b^{-1})$ corresponds to the near forward endfire beam.
- For $f_k < f_d$ Eq. (3) gives $\sin\theta_n$ outside of $[-1,1]$, the corresponding beam wavenumbers are not related to a real acoustic direction and are commonly termed virtual beams; conversely those lying in the real acoustic region are termed real beams.

2.2. HIGH-RESOLUTION BEAMFORMER

In most high-resolution methods some *a priori* information is required on the form of the model for the field generating process and/or for the estimation of the model parameters. Mismodeling and sub-optimum parameter estimation are very often confused in the real case.

To avoid these problems a different solution was proposed by Wagstaff et al., the Wagstaff–Berrou broadband (WB^2) algorithm [8]. In this report we shall use a modified version of this algorithm due to J.-L. Berrou (WB^3); for convenience the algorithm equation flowchart is given in the appendix. Here we will simply recall the basic ideas of the WB techniques.

In the WB algorithms noise field estimation is considered as an inverse problem with the conventional beamformer estimate as input. The WB algorithms are based on the assumption that the acoustic field incident on the array can be described as a sum of uncorrelated plane waves with wavenumber values κ_i, $i = 1, \ldots, N_h$. Thus the mean of the conventional beamformer output at time t, frequency f_k and wavenumber κ_n can be expressed by the discrete wavenumber convolution relationship

$$\hat{B}(f_k, n, t) = E[B(f_k, \kappa_n, t)] = N_h^{-1} \sum_{i=0}^{N_h-1} P_{n-i} F_i, \quad n = 1, \ldots, N_b, \tag{4}$$

where $F_i = F(f_k, \kappa_i, t)$ with $i = 1, \ldots, N_h$ is the discrete wavenumber spectrum given by a hypothetical array of $N_h \gg N_b$ sensors with the same hydrophone spacing as the actual array and P_{n-i} is the wavenumber spectrum of the spatial shading function $h(l)$, i.e.

$$P_i = \left| \sum_{l=0}^{N_b - 1} h(l) \exp[j 2\pi \kappa_i l] \right|^2, \quad i = 1, \ldots, N_h - 1, \tag{5}$$

evaluated at the point $n - i$. The basic idea (knowing the array beampattern P_i) is to deconvolve the discrete wavenumber spectrum F_i from the measured conventional beamformer beamnumber spectrum $\hat{B}(f_k, n, t)$. In the WB algorithms all the spectrum quantities are expressed in a decibel scale which emphasizes the importance of the low acoustic levels and facilitates the estimation of low-level sources in the presence of high-level noise sources [8]. The computer implementation of the algorithm is somewhat simplified by this decibel notation but the inverse problem turns out to be highly nonlinear. Also, as the number N_h of discrete values of the field F_i is much larger than the number of beams N_b, the inversion of (4) leads to an indetermination of minimum order $N_h - N_b$.

The WB algorithms give an approximate solution to this problem by means of a gradient iterative technique based on the minimization, at each iteration k, of the mean square error between the predicted beamformer response (4) for the kth iteration discrete wavenumber spectrum F_i^k and the actual measured beamformer response.

The main differences between the original algorithm (WB^2) and the actual algorithm (WB^3) consists in the first guess of the field F_i^0 and the correction applied at each iteration to pass from F_i^k to F_i^{k+1}. The iteration process is stopped either when the mean square error passes below a given threshold or when a given fixed number of iterations has been reached.

The WB^2 high-resolution algorithm was qualitatively shown to give similar results to the majority of well-known high-resolution techniques [8]. A simulated comparative quantitative study of resolution, detection and accuracy performance is given in [9].

3. Methodology of detection

The purpose of this section is to describe the detection procedure adopted to carry out a statistically significant signal detection study comparing the conventional planewave beamformer and the high-resolution beamformer on a real ship-induced environment.

This study is restricted to the test of presence or absence of a single narrow-band signal (target) when the direction and frequency signature are known. Standard detection procedures normally use a frequency–azimuth display and the assumption that the frequency bins apart from the signal frequency are noise-only frequencies. These noise-only frequency bins are then averaged to produce an estimate of the mean noise power. In this case, the detection problem leads to a simple conventional testing against a given power threshold based on the previous estimated mean noise power.

For the database discussed in this report, frequency–wavenumber estimates are obtained for 256 discrete frequencies ranging from 112.5 Hz to 750 Hz at 2.5 Hz increments. Each surface is obtained for an averaging time of slightly less than 3 min; N_b = 128 beams were formed which is twice the number of hydrophone elements; Hann shading was used both in time-to-frequency and hydrophone-to-wavenumber transforms. For testing purposes a multitone controlled source emitted from a known location about 75 n.mi away from the measurement site was used as a target. The controlled source input spectrum is formed by a number of CW lines ranging from 133.33 Hz to 600 Hz with a frequency increment of 33.33 Hz and variable power level. A reference peak is located at the frequency of 500 Hz which is used as reference for source azimuth estimation. The five lowest frequency lines were used as test signals in this study (see Table 1).

Let us define as 'signal frequencies' the discrete frequencies of the frequency–wavenumber spectrum estimates that are close to the source CW line frequencies (see Table 1). By assumption the other frequencies will be called the 'noise-only frequencies'.

For detection and false alarm probabilities estimation a detection is obtained whenever a line is detected at a 'signal frequency', and a false alarm is obtained whenever a line is detected at a 'noise-only frequency'. Thus, the empirical estimates of the detection probability $\mathcal{P}_d$ and the false alarm probability $\mathcal{P}_{fa}$ are respectively given by

$$\hat{\mathcal{P}}_d = \frac{\text{number of line detections at signal frequency}}{\text{total number of estimates}}, \tag{6a}$$

Table 1
Transmitted source signal characteristics

Source frequencies (Hz)	Relative power (dB)	Discrete frequencies (Hz)
133.33	-55.28	132.50
166.66	-40.23	167.50
200.00	-42.60	200.00
233.33	-40.30	232.50
266.66	-36.10	267.50

$$\hat{P}_{f,\theta} = \frac{\text{number of line detections at noise-only frequency}}{\text{total number of estimates}}. \tag{6b}$$

For the conventional planewave beamformer estimate one can define the simplest detection test by

$$\hat{B}(f_k, \theta_s, t_j) \geq \gamma_j, \tag{7}$$

where f_k may be a signal or a noise-only frequency, depending upon whether we estimate the detection probability or the false alarm probability; θ_s is the source azimuth beam steering angle and t_j is the discrete time at which the estimate was obtained.

For the high-resolution WB^3 beamformer the detection test is defined by the expression

$$\mathrm{MF}(f_k, \theta_s, t_j) \geq \gamma_j^{\mathrm{dB}}, \tag{8}$$

where $\mathrm{MF}(f_k, t_j)$ is defined as the maximum level (expressed in dB) of the WB^3 field estimate within the width of the conventional planewave beamformer mainlobe at the considered discrete frequency f_k and for the source signal beam steering angle θ_s. The detection threshold γ_j^{dB} is simply γ_j expressed in dB.

In (7) γ_j is the mean noise power 'background' dependent threshold at time t_j. In practice the noise power 'background' may be estimated either by an average of a number of 'noise-only frequency' bins in the signal direction or by an average of the noise levels in contiguous beam steering directions at a noise-only frequency, or even some combination of both estimates. In the general case the detection threshold is given by

$$\gamma_j = \gamma_T + \frac{1}{LQ} \sum_{l=1}^{L} \sum_{q=1}^{Q} \mathcal{L}(f_l, \theta_q, t_j), \tag{9}$$

where L is the number of noise-only frequency bins and Q is the number of contiguous beams; γ_T is a variable detection threshold depending on the false alarm rate for a

fixed signal-to-noise ratio. In (9) the symbol $\mathcal{L}$ stands for the conventional or the WB[3] high-resolution beamformer level (at the specified frequency, steering angle and time) depending on whether a conventional or high-resolution detection test is being performed.

The results are shown in the form of a series of receiver operating characteristics (ROC) curves, i.e. estimated $\mathcal{P}_d$ as a function of estimated $\mathcal{P}_{f_a}$ for variable detection threshold γ_T, for the lowest signal frequencies of the source signal (see Table 1).

4. Results

The high-resolution database used in this study is composed of about 6 h of array data recording which provides a total of 120 frequency-wavenumber estimates. The sampling frequency is F_s = 2560 Hz for an FFT block size of N_s = 1024. The number of averages (time-bandwidth product) is N = 60. Figure 1 shows an example of a conventional beamformer output (a) and the respective WB high-resolution estimate (b) for a frequency f_s = 200 Hz.

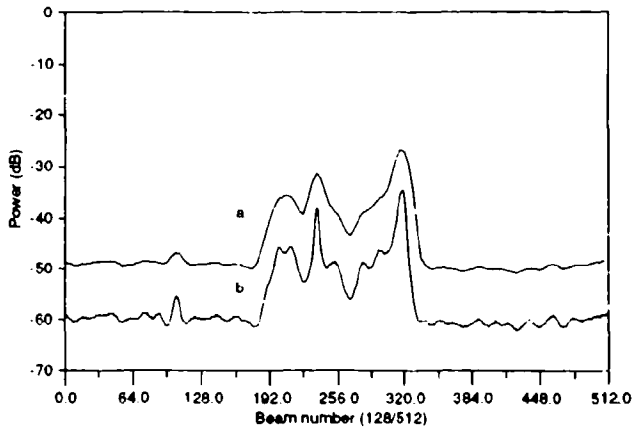

Fig. 1. Conventional beamformer (a) and WB high-resolution (b) estimates: number of beams N_b = 128 (a) and N_b = 512 (b); number of averages N = 150, frequency f_s = 200 Hz.

Results are presented as a series of five empirical ROC curves (percentage of detection *vs* percentage of false alarms) for a threshold variation $\gamma_{min} \leq \gamma_T \leq \gamma_{max}$:

$$\gamma_{min} = 0.316 \quad (= -5 \text{ dB}),$$

$$\gamma_{max} = 2.81 \quad (= 4.5 \text{ dB}).$$

There are a total number of 40 discrete points on each ROC curve. In practice the values L = 3 and Q = 3 were chosen for the expression of the mean noise power

estimator of (10). The three noise-only frequencies were chosen one below the signal frequency, one between the signal and the noise frequencies, and one above the noise frequency. The five signal frequencies in Table 1 (132.5, 167.5, 200.0, 232.5 and 267.5 Hz) have been processed giving the results shown in Figs. 2-6. To facilitate comparison the ROC curves of both the conventional planewave beamformer and the high-resolution beamformer are plotted on each figure.

For the four lowest frequency lines (f_s = 132.5, 167.5, 200 and 232.5 Hz) the conventional beamformer showed a relatively poor performance, only slightly better than the chance diagonal defined by $P_d = P_f$. For these frequencies the detection performance of the high-resolution beamformer is from 5% to 20% larger than that achieved by the conventional beamformer. Note that this improvement was obtained for the range of false alarm rates of most interest to us, i.e. for $5\% \leq P_f \leq 40\%$.

For the highest level line (f_s = 267.5 Hz) the performance of the two beamformers is comparable, attaining relatively high detection probability rates for the same false alarm probability range.

These results suggest that the poor performance of the conventional plane-wave beamformer for the lowest frequencies is due not only to the low signal-to-noise ratio of the signal under detection but also to a lack of resolving power. This lack of resolving power could be, at least partially, recovered by using a high-resolution beamformer giving rise to an increase in detection performance without increasing the array aperture.

When operating at the highest frequencies, where the signal-to-noise ratio and the resolving power are higher, the two beamformers gave the same detection performance.

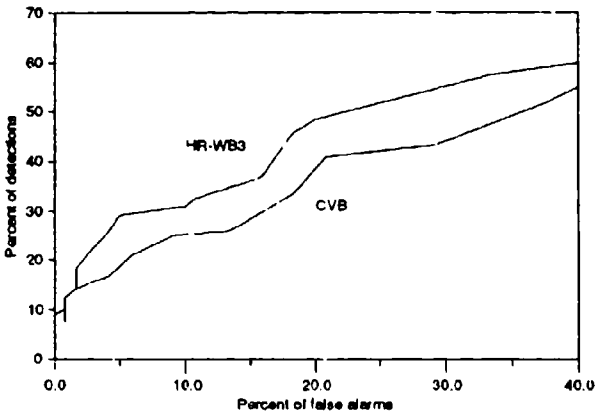

Fig. 2. Empirical ROC curves of the conventional and high-resolution beamformer for frequencies f_s = 132.5 Hz and f_n = 150 Hz.

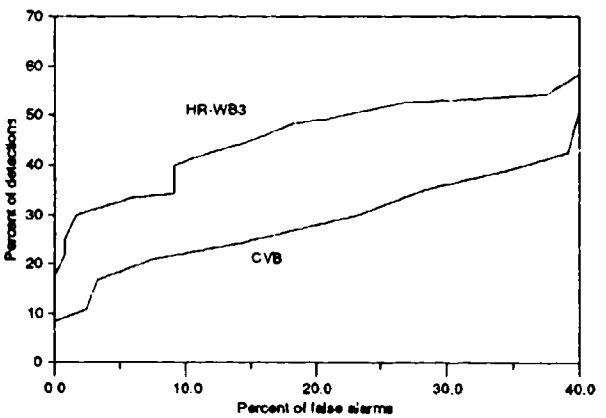

Fig. 3. Empirical ROC curves of the conventional and high-resolution beamformer for frequencies f_s = 167.5 Hz and f_n = 182.5 Hz.

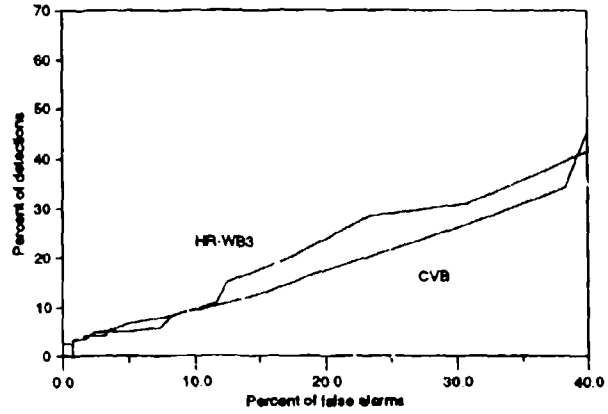

Fig. 4. Empirical ROC curves of the conventional and high-resolution beamformer for frequencies f_s = 200 Hz and f_n = 215 Hz.

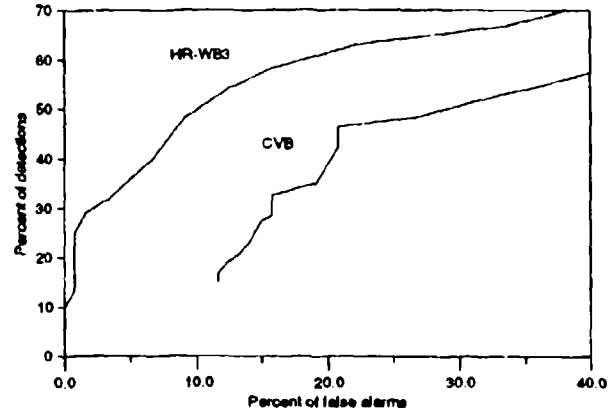

Fig. 5. Empirical ROC curves of the conventional and high-resolution beamformer for frequencies f_s = 232.5 Hz and f_n = 250 Hz.

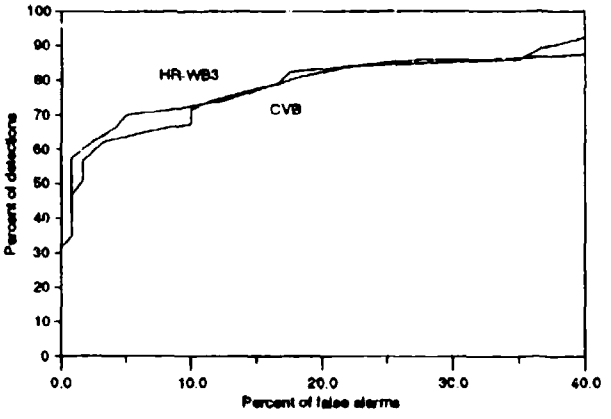

Fig. 6. Empirical ROC curves of the conventional and high-resolution beamformer for frequencies f_s = 267.5 Hz and f_n = 282.5 Hz.

5. Conclusion

In this report the results of the detection of a low-level narrow-band signal in real coherent ship-induced noise are presented. The detection performance behaviour of both the conventional beamformer and a high-resolution beamformer (WB algorithm) are shown under the form of ROC curves for different frequencies and signal-to-noise ratio.

The results obtained on this particular set of data, acquired during July 1984 in the Gulf of Genova, show that a significant detection improvement can be achieved by high-resolution data processing for the lowest signal-to-noise ratio. This improvement ranges from 5% to 20% depending on the allowed false alarm rate and on the signal-to-noise level considered. For the highest signal-to-noise ratio the performance of the two beamformers was comparable.

These results suggest that for acoustic fields dominated by a multi-source noise structure, the use of a high-resolution beamformer may lead to an improvement of the detection performance of conventional sonar systems. This detection improvement is due to the ability of the high-resolution beamformer to resolve the signal in the presence of such a multi-source structure. In this case high-resolution beamforming represents a potential candidate for low-level target detection with short aperture arrays. A real life example of such a situation was shown in this study for an acoustic field dominated by ship traffic noise.

However, further work is needed to enlarge the statistical significance of the results obtained here to other databases acquired in various sites and with different ship distributions. Possibly, well-adapted high-resolution techniques can be designed to include *a priori* noise field coherence characteristics in order to achieve higher detection performances in ship-induced noise fields.

References

[1] CAPON, J. High-resolution frequency-wavenumber spectrum analysis. *Proceedings of the IEEE* **57**, vol. 8, 1969: 1408–1418.

[2] BURG, J.P. Maximum entropy spectral analysis. PhD. Dissertation. Stanford University, 1975.

[3] PISARENKO, V.F. The retrieval of harmonics from a covariance function. *Geophysical Journal of the Royal Astronomical Society*, **33**, 1973: 347–366.

[4] SCHMIDT, R.O. A signal subspace approach to multiple emitter location and spectral estimation. PhD. Dissertation. Stanford University, 1982.

[5] BIENVENU, G. Influence of the spatial coherence of the background noise on high-resolution passive methods. *In*: INSTITUTE OF ELECTRICAL AND ELECTRONICS ENGINEERS. IEEE ACOUSTICS, SPEECH AND SIGNAL PROCESSING SOCIETY. IEEE International Conference on Acoustics, Speech and Signal Processing, ICASSP 79, Washington, D.C., 2-4 April, 1979. Piscataway, NJ, IEEE, 1979: pp 306–309. [79CH1379-7 ASSP].

[6] ZIMMER, W.M.X. High-resolution beamforming techniques performance analysis, SACLANTCEN SR-104. La Spezia, Italy, SACLANT Undersea Research Centre, 1986. [AD A 179 060]

[7] WAGSTAFF, R.A. Iterative technique for ambient-noise horizontal-directionality estimation from towed line-array data. *Journal of the Acoustical Society of America*, **63**, 1978: 863–869.

[8] WAGSTAFF, R.A. and BERROU, J.-L. A fast and simple nonlinear technique for high-resolution beamforming and spectral analysis *Journal of the Acoustical Society of America*,**75**, 1984: 1133–1141.

[9] ZIMMER, W.M.X. Logarithmic least mean square sound-field estimation, SACLANTCEN SR-110. La Spezia, Italy, SACLANT Undersea Research Centre, 1987. [AD A 180 587]

Appendix A

WB³ algorithm equation flowchart

The following notation is used: All quantities in capital letters are defined in decibels. N_b is the number of beams on the conventional planewave beamformer, and N_h is the number of beams on the high-resolution field estimate; in practice $N_h = 4N_b$. The quantity BW_n is defined as the nth conventional beamwidth.

Step 1 Get the measurements:

$$\{B_n\}, \qquad n = 1, \ldots, N_b.$$

Step 2 Get array beampattern:

$$\{H_i\}, \qquad i = 1, \ldots, N_h.$$

Step 3 Get first field estimate, $k = 0$:

$$F_i^k = \min_n [B_n - H_{n-i} - 10\log(BW_n)], \qquad i = 1, \ldots, N_h.$$

Step 4 Get predicted beamformer response to field F^k:

$$\hat{B}_n(F^k) = 10\log\left[\sum_{i=1}^{N_h} 10^{(F_i^k + H_{n-i})/10}\right].$$

Step 5 Compute dB error:

$$DE(B, F^k) = \sum_{n=1}^{N_b} \left[B_n - \hat{B}_n(F^k)\right]^2.$$

Step 6 Stop iteration test on dB error:

If $DE(B, F^k) \leq DE_0$ then stop, otherwise go to Step 7.

Step 7 Update field estimate:

$$F_i^{k+1} = F_i^k + C_i(B, F^k), \qquad i = 1, \ldots, N_h,$$

with the correction

$$C_i(B, F^k) = w_i \frac{\sum_{n=1}^{N_b} \left[B_n - \hat{B}_n(F^k) \right] \mathrm{IMP}_{n,i}^c}{\sum_{n=1}^{N_b} \mathrm{IMP}_{n,i}^c},$$

where c is a constant generally set to 1.5 or 2 and

$$\mathrm{IMP}_{n,i} = 10^{\left[F_i^k - H_{n-1} - \hat{B}_n(F^k) \right]/10},$$

$$w_i = \min\left[1, \mathrm{TIMP}_i/\mathrm{AVIMP}_i\right],$$

where

$$\mathrm{TIMP}_i = \sum_{n=1}^{N_b} \mathrm{IMP}_{n,i}$$

and AVIMP_i is defined as TIMP_i for a flat field, i.e. F_i = constant.

Step 8 Stop test on the number of iterations:

If $k = k_0$ then stop, otherwise increment $k = k + 1$ and go to Step 4.

Initial Distribution for SR-144

Ministries of Defence	
JSPHQ Belgium	2
DND Canada	10
CHOD Denmark	8
MOD France	8
MOD Germany	15
MOD Greece	11
MOD Italy	10
MOD Netherlands	12
CHOD Norway	10
MOD Portugal	2
MOD Spain	2
MOD Turkey	5
MOD UK	20
SECDEF US	68
NATO Authorities	
Defence Planning Committee	3
NAMILCOM	2
SACLANT	3
SACLANTREPEUR	1
CINCWESTLANT/ COMOCEANLANT	1
COMSTRIKFLTANT	1
CINCIBERLANT	1
CINCEASTLANT	1
COMSUBACLANT	1
COMMAIREASTLANT	1
SACEUR	2
CINCNORTH	1
CINCSOUTH	1
COMNAVSOUTH	1
COMSTRIKFORSOUTH	1
COMEDCENT	1
COMMARAIRMED	1
CINCHAN	3
SCNR for SACLANTCEN	
SCNR Belgium	1
SCNR Canada	1
SCNR Denmark	1
SCNR Germany	1
SCNR Greece	1
SCNR Italy	1
SCNR Netherlands	1
SCNR Norway	1
SCNR Portugal	1
SCNR Turkey	1
SCNR UK	1
SCNR US	2
French Delegate	1
SECGEN Rep. SCNR	1
NAMILCOM Rep. SCNR	1
National Liaison Officers	
NLO Canada	1
NLO Denmark	1
NLO Germany	1
NLO Italy	1
NLO UK	1
NLO US	1
NLR to SACLANT	
NLR Belgium	1
NLR Canada	1
NLR Denmark	1
NLR Germany	1
NLR Greece	1
NLR Italy	1
NLR Netherlands	1
NLR Norway	1
NLR Portugal	1
NLR Turkey	1
NLR UK	1
Total external distribution	250
SACLANTCEN Library	10
Stock	20
Total number of copies	280